Maximum Voltage Utilization of IPMSMs Using Modulating Voltage Scalability for Automotive Applications

SeHwan Kim, *Student Member, IEEE*, and Jul-Ki Seok, *Senior Member, IEEE*

***Abstract*—A hybrid maximum voltage utilization controller is developed for interior permanent-magnet synchronous motors over a wide operating range. The structure of the controller combines the current vector control (CVC)-type maximum torque per ampere controller and the modulating voltage-scaled controller (MVSC). The hybrid structure provides a smooth transition from the CVC to the proposed MVSC mode by deactivating the current regulator in the flux weakening region. A seamless transition to a full six-step modulation can be realized by adjusting the scaling gain, which is a significant merit in terms of power utilization for wide flux weakening applications. This paper also examines the torque control accuracy under motor parameter drifts to determine how to decouple its effect using a voltage disturbance state-filter design.**

***Index Terms*—Full six-step modulation, hybrid maximum voltage utilization controller, interior permanent-magnet synchronous motors (IPMSMs) over a wide operating region, modulating voltage-scaled controller (MVSC), voltage disturbance state filter.**

I. Introduction

INTERIOR permanent-magnet synchronous motors (IPMSMs) have attracted considerable attention in the field of automotive traction applications owing to their high efficiency, high power density, and a wide constant power speed range [1]–[3]. The extension of dc-link voltage utilization is one important issue in these wide flux-weakening ranges that is relevant to the control of IPMSMs because high efficiency or minimum copper loss operation is crucial due to the limited battery power [4]–[6]. A number of methods for exploiting the available bus voltage have been reported over a wide range of speeds based on current vector control (CVC) [7], [8]. With CVC-based methods, however, the maximum voltage utilization is not realized because they consider the voltage limit as a circle instead of a hexagon limit. A modified CVC methodology was proposed [9] to extend the linear voltage limit to the quasi-six-step range. Although this solution uses a more allowable voltage than that of conventional CVC methods, it does not utilize the "true" maximum voltage because the controller should always maintain a certain voltage for current regulation. This suggests that the modified CVC method cannot achieve the true maximum voltage utilization but accomplish only "near" maximum voltage utilization. Moreover, these approaches are unable to reach the full six-step mode due to the current control instability.

This paper presents the design and implementation of a hybrid maximum voltage utilization controller for achieving power density enhancement over a wide operating region. The CVC-type maximum torque per ampere (MTPA) control is used to retain the minimum copper loss operation under the base speed. The motor control is handed over to the proposed modulating voltage-scaled controller (MVSC) at the voltage limits. In particular, the current regulator is deactivated to achieve the true maximum voltage utilization in the MVSC region. This can be implemented easily by scaling a modulating voltage, which leads to a simple structure. The proposed control provides a smooth transition between CVC operation and MVSC mode. In addition, a seamless transition to the full six-step modulation can be realized by simply adjusting the scaling gain because no current control is used in the MVSC mode. This paper also examines the torque control accuracy under motor parameter drifts to determine how to decouple its effect using a voltage disturbance state filter. A comprehensive collection of experiments are conducted to evaluate the feasibility of the presented idea.

II. Analysis and Design of the Maximum Voltage Utilization Controller

A. Design of a Modulating Voltage-Scaled Controller

Fig. 1 shows a block diagram of the proposed hybrid maximum voltage utilization control strategy for an IPMSM using a complex vector representation. Here, $\mathbf{v}_{dq}$ and $\mathbf{i}_{dq}$ are the $d-q$-axis stator voltage and current vector in the rotor reference frame, respectively. R_s represents the stator resistance, ω_r is the rotor angular velocity, $V_{\rm dc}$ indicates the measured dc-link voltage, and $\mathbf{J} = \begin{bmatrix} 0 & -1 \\ 1 & 0 \end{bmatrix}$. The stator inductance and the magnet flux linkage can be defined as

$$\mathbf{L}_s = \begin{bmatrix} L_d & 0 \\ 0 & L_q \end{bmatrix} \text{ and } \mathbf{\Lambda}_{\rm pm} = \begin{bmatrix} \lambda_{\rm pm} \\ 0 \end{bmatrix} \tag{1}$$

where L_{dq} is the *d*–*q*-axis stator inductance and $\lambda_{\rm pm}$ is the flux linkage of the permanent magnet. The command torque T_e^* and inverse command flux $\frac{\sqrt{3}\omega_r}{V_{\rm dc}}\left(=\lambda_s^{-1^*}\right)$ are considered inputs

Manuscript received October 31, 2012; revised January 24, 2013; accepted March 17, 2013. Date of current version June 6, 2013. This work was supported by the National Research Foundation of Korea under a grant funded by the Korea Government (MEST) (2012-0009148). Recommended for publication by Associate Editor B. Sarlioglu.

The authors are with the School of Electrical Engineering, Yeungnam University, Gyeongsan, Gyeongbuk 712-749, Korea (e-mail: ksh_8508@ynu.ac.kr; doljk@ynu.ac.kr).

Color versions of one or more of the figures in this paper are available online at http://ieeexplore.ieee.org.

Digital Object Identifier 10.1109/TPEL.2013.2253802

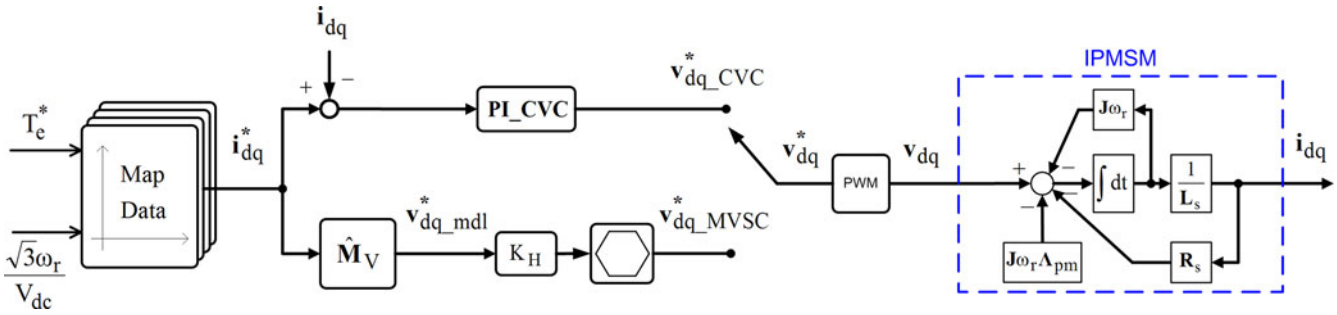

Fig. 1. Proposed hybrid controller for maximum voltage utilization.

to the map data block, which is often constructed from multidimensional lookup tables to cover the MTPA and flux weakening operation [10], [11]. Therefore, the map data blocks are mapped to generate the *d–q*-axis current commands $\mathbf{i}^*_{dq}$ with respect to the linear voltage limit for CVC purposes [9]. The map data are generated by steady-state measurements of motor voltages, currents, dc-link voltage, rotor speed, and real torque at various temperatures and operating conditions. Thus, the map blocks can be assumed to be accurate to represent a real motor because they are sufficiently large to cover saturation nonlinearities in the operating space and robust against the thermal variations by the motor temperature feedback or estimation [12].

The stator current $\mathbf{i}_{dq}$ is controlled by a familiar proportional-integral-type current regulator (PI_CVC) to track the command current vector $\mathbf{i}^*_{dq}$. The command voltage vector $\mathbf{v}^*_{dq\_\mathrm{CVC}}$ by current control is transferred to the IPMSM within the voltage limit.

At high speeds, however, the command voltage $\mathbf{v}^*_{dq\_\mathrm{mdl}}$ can be calculated using the rotor reference frame-based voltage model $\hat{\mathbf{M}}_V$ as follows:

$$\mathbf{v}^*_{dq\_\mathrm{mdl}} \cong \omega_r \mathbf{J}\hat{\mathbf{L}}_s \mathbf{i}^*_{dq} + \omega_r \mathbf{J}\hat{\mathbf{\Lambda}}_{\mathrm{pm}}. \tag{2}$$

In this paper, superscript "^" represents the corresponding variables that are estimated and superscript s is used to denote a stationary reference frame. Note that $\mathbf{v}^{s^*}_{dq\_\mathrm{mdl}}$ always remains within the linear voltage limit with a radius of $\frac{V_{\mathrm{dc}}}{\sqrt{3}}$ because it is calculated from a CVC-based command current $\mathbf{i}^*_{dq}$, as shown in Fig. 2. To extend the voltage utilization to the hexagon limit, the modulating voltage $\mathbf{v}^{s^*}_{dq\_\mathrm{mdl}}$ is increased to the outside of the hexagon by multiplying the scalar gain K_H, while minimizing the torque discontinuity. These infeasible voltages are then scaled back to the hexagon voltage limit using the minimum magnitude-error overmodulation with a simple switching time manipulation [13], [14]. An increase in K_H leads to the convergence of the scaled voltage vector $\mathbf{v}^{s^*}_{dq\_\mathrm{MVSC}}$ around the tip of the hexagon. As a result, the transition to full six-step modulation can be achieved by gradually amplifying K_H. To justify this assertion, Fig. 3 gives an example of the IPMSM, described in Table I in the MVSC mode, under a half-rated torque condition while the motor operates at 114% of the base speed. The scaled A-phase voltage command $\mathbf{v}^*_{\mathrm{as\_MVSC}}$ moves to full

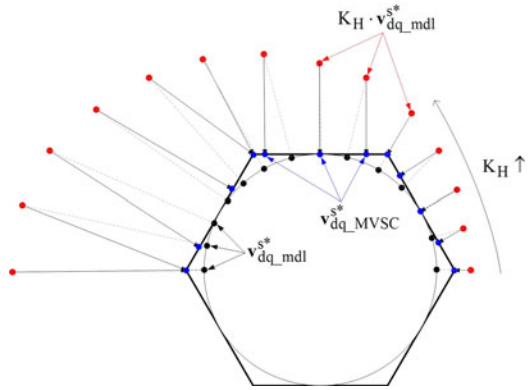

Fig. 2. Minimum magnitude-error overmodulation for modulating voltage scalability.

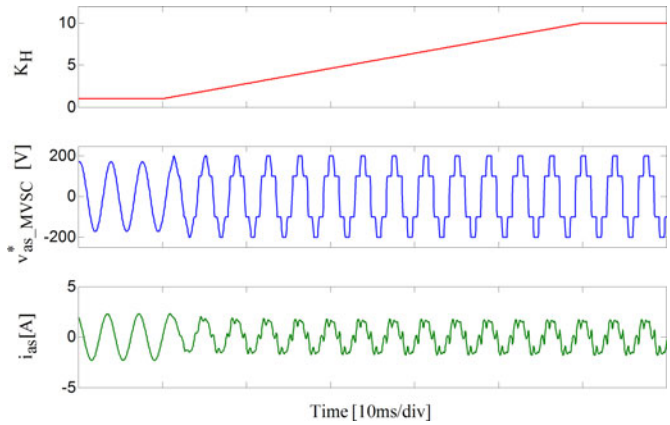

Fig. 3. Transition into the full six-step modulation with K_H.

six-step modulation and the current i_{as} becomes distorted as the scalar gain K_H increases gradually.

Note that a rapid change of K_H may result in torque oscillations. To avoid this situation, the change rate of K_H, delivering the voltage from maximum linear modulation region $\left(\frac{V_{\mathrm{dc}}}{\sqrt{3}}\right)$ to six-step modulation $\left(\frac{2V_{\mathrm{dc}}}{3}\right)$, must be lower than $\frac{2/3}{1/\sqrt{3}} f_{\mathrm{rpm}}$, where f_{rpm} is the mechanical rotor angular frequency in r/min, as shown in Fig. 4.

TABLE I
RATINGS AND NOMINAL PARAMETERS OF 900-W IPMSM UNDER TEST

Ratings and Parameters	Value	Unit
Rated torque	2.9	Nm
Number of poles	8	
Base speed@150 V_{dc}	1700	r/min
L_d	8.5	mH
L_q	20.2	mH
λ_{pm}	0.115	Wb

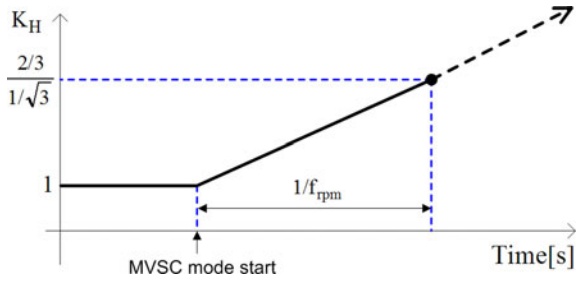

Fig. 4. Minimum change rate of K_H.

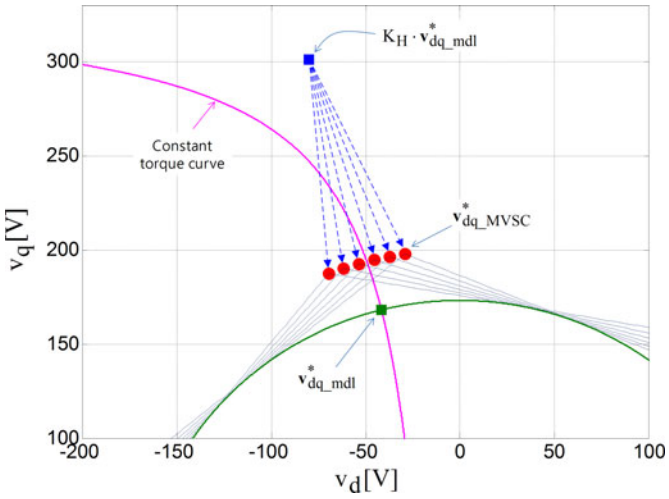

Fig. 5. Torque control principle in the MVSC mode.

B. Analysis of a Modulating Voltage-Scaled Controller

To obtain better insight into the principle of torque control for the proposed MVSC structure, scaled command voltage vectors were displayed for a constant torque curve in the synchronous d–q volt plane, as shown in Fig. 5. With the minimum magnitude-error overmodulation, the motor torque was regulated around the desired torque curve using $\mathbf{v}^*_{dq\_\mathrm{MVSC}}$ (marked in red dots). This may cause fluctuations in the generated torque, which might not be severe or problematic, for automotive applications requiring the maximum voltage excitation because high-order harmonics are almost filtered out at these high speeds.

In this paper, a smooth transition could be achieved simply by resetting the CVC integrator at the mode switching instant. The performance is confirmed by an acceleration and deceleration test, as illustrated in Fig. 6, where the rotor speed, real motor torque, and q-axis integrator term of the PI_CVC are depicted from the top to bottom. The transition base speed was set to 3500 r/min. Distortions were rarely found during the transition, which can lead to a smooth transition with no abrupt changes in motor torque.

Fig. 7 shows the stator current vector trajectories in the d–q current plane for the different torque requirements. The stator current vector in the CVC mode slides on the constant torque curve during the mode transition while its magnitude $|\boldsymbol{i}_{dq\_\mathrm{MVSC}}|$

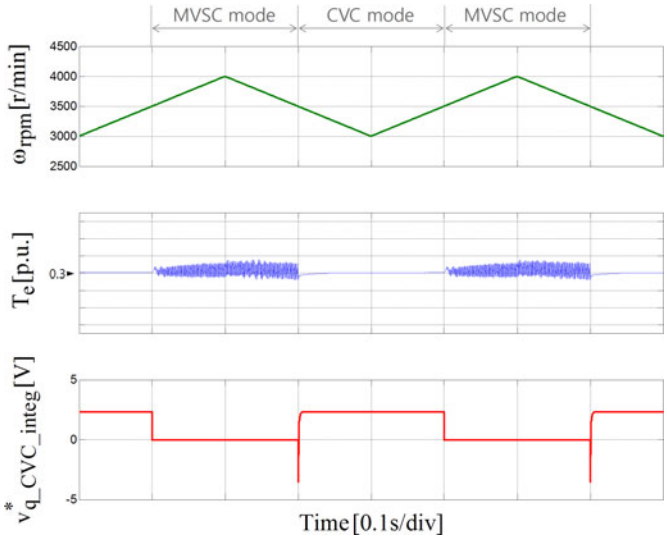

Fig. 6. Control mode switching of the proposed hybrid structure.

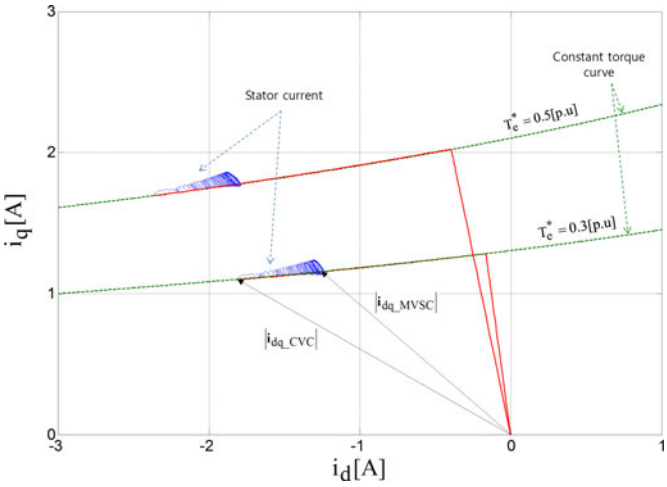

Fig. 7. Voltage trajectory between CVC and MVSC modes in the d–q current plane.

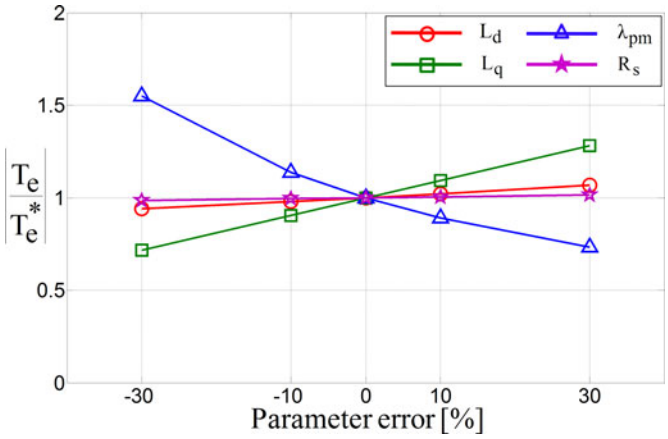

Fig. 8. Torque control accuracy by motor parameter drifts in the MVSC mode at 1.3 p.u. of the base speed.

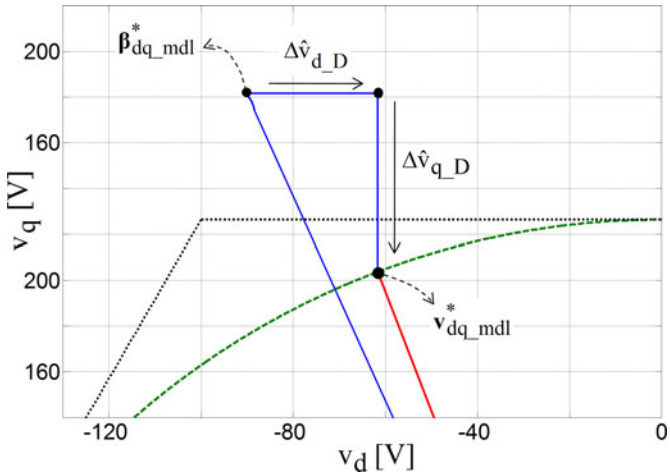

Fig. 9. Voltage deviation effect resulted from parameter drifts.

is reduced in the MVSC mode owing to the maximum voltage utilization. Using the proposed hybrid voltage control, the minimum copper loss operation is achieved over the entire operating range.

C. Compensation of Effects of Parameter Drifts

In practice, the precise torque regulation is not trivial in the MVSC mode because the machine parameters of (2) drift due to high saturation and PM flux variations with temperature, as shown in Fig. 8. Note that the stator resistance error has little impact on torque control at high speeds. Two primary approaches have been competing to cure this problem. One method is to construct multidimensional or numerous inverse model maps based on steady-state measurements of the motor voltage, currents, dc-link voltage, rotor speed, and real torque. In addition to the multidimensional map data blocks, these lookup tables cause add-on reliance on large memory and time-consuming tests.

In practical applications, online compensation for model errors is believed to be more effective in achieving accurate torque control. This paper proposes a voltage disturbance state filter [15], [16] to decouple the parameter dependence of the MVSC mode.

When there are variations in the parameters, as shown in Fig. 9, the command voltage $\mathbf{v}^*_{dq\_\mathrm{mdl}}$ in the d–q volt plane deviates from the linear voltage limit to $\boldsymbol{\beta}^*_{dq\_\mathrm{mdl}}$ according to the following equation:

$$\boldsymbol{\beta}^*_{dq\_\mathrm{mdl}} \cong \omega_r \mathbf{J}\hat{\mathbf{L}}_s \mathbf{i}^*_{dq} + \omega_r \mathbf{J}\hat{\boldsymbol{\Lambda}}_{\mathrm{pm}}. \tag{3}$$

Here, $\Delta\hat{v}_{d\_D}$ represents the d-axis voltage deviation resulting from the error of $\hat{L}_q$. The part of the circle (in green) indicates the linear voltage limit.

The $\boldsymbol{\beta}^*_{dq\_\mathrm{mdl}}$ deviation causes $\mathbf{v}^*_{dq\_\mathrm{MVSC}}$ to migrate from the associated reference trajectory on the hexagon, which is a primary source of torque errors in Fig. 8. The purpose is to determine the disturbance voltage orienting $\boldsymbol{\beta}^*_{dq\_\mathrm{mdl}}$ toward $\mathbf{v}^*_{dq\_\mathrm{mdl}}$ on the linear voltage limit circle. In the open-loop MVSC mode,

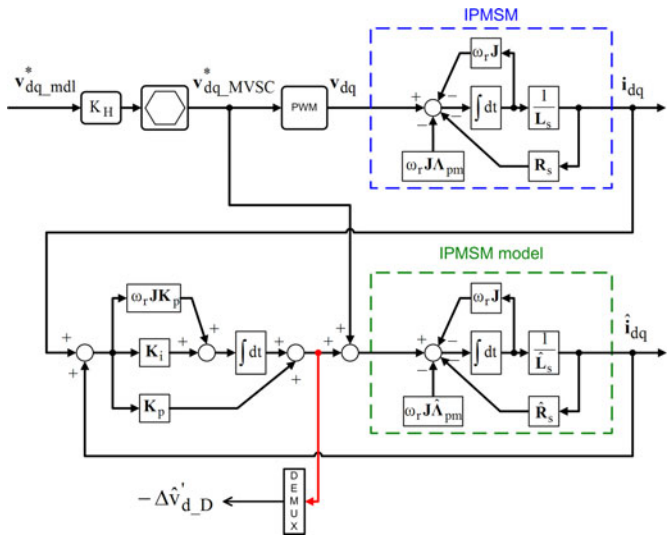

Fig. 10. Modified state-filter design for decoupling the parameter dependence in the MVSC mode.

the standard state-filter structure cannot capture the disturbance voltage resulting from parameter drifts because it is designed for closed-loop current regulator [15], [16]. This leads to a modified state-filter design that identifies the d- and q-axis voltage deviation separately.

Fig. 10 shows the modified state filter for the d-axis voltage disturbance estimation where the estimated output current $\hat{\mathbf{i}}_{dq}$ follows the motor current $\mathbf{i}_{dq}$. Therefore, at high speeds, the d-axis disturbance voltage can be obtained from the following equation:

$$\Delta\hat{v}'_{d\_D} \cong -\omega_r \Delta L_q i_q \tag{4}$$

where $\Delta L_q = \hat{L}_q - L_q$. The d-axis voltage deviation term can then be computed as

$$\Delta\hat{v}_{d\_D} = -\Delta\hat{v}'_{d\_D} \times \frac{i^*_q}{i_q} = \omega_r \Delta L_q i^*_q. \tag{5}$$

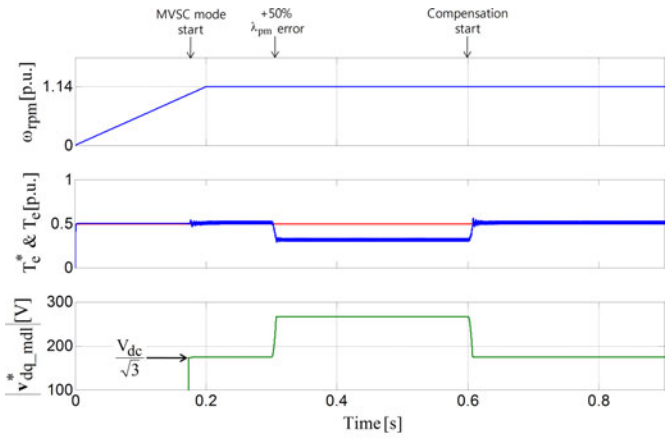

(a)

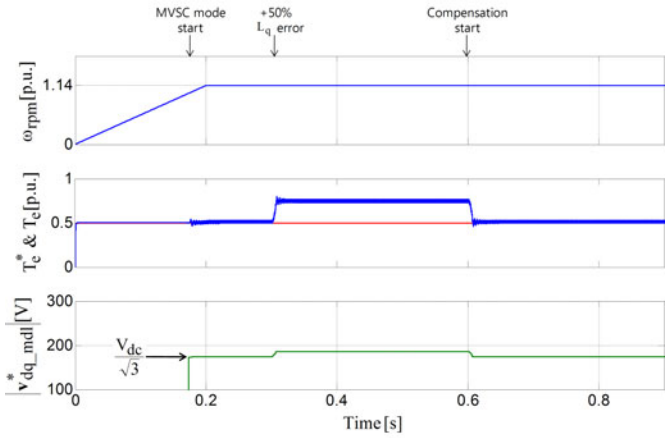

(b)

Fig. 11. Torque compensation results. (a) $+50\%\ \Delta\lambda_{\rm pm}$. (b) $+50\%\ \Delta L_q$.

With the compensation of (5), as shown in Fig. 9, the d-axis component of $\boldsymbol{\beta}^*_{dq\_\rm mdl}$ coincides with that of $\mathbf{v}^*_{dq\_\rm mdl}$ as follows:

$$\begin{aligned}\boldsymbol{\beta}^*_{d\_\rm mdl} + \Delta\hat{v}'_{d\_D} &= -\omega_r\left(\hat{L}_q i^*_q - \Delta L_q i^*_q\right)\\ &= -\omega_r L_q i^*_q = v^*_{d\_\rm mdl}.\end{aligned} \tag{6}$$

Once $v^*_{d\_\rm mdl}$ is identified correctly, as shown in Fig. 9, $\Delta\hat{v}_{q\_D}$ resulted from ΔL_d and $\Delta\lambda_{\rm pm}$ can be automatically obtained because $\mathbf{v}^*_{dq\_\rm mdl}$ is always on the voltage circle with a radius of $\frac{V_{\rm dc}}{\sqrt{3}}$. Then, $v^*_{q\_\rm mdl}$ becomes

$$v^*_{q\_\rm mdl} = \mathrm{sgn}\left(\omega_r\right)\cdot\sqrt{\left(\frac{V_{\rm dc}}{\sqrt{3}}\right)^2 - v^{*2}_{d\_\rm mdl}}. \tag{7}$$

Fig. 11 shows the simulated compensation results of the parameter variation effect at 114% of the base speed and a half-rated torque command. The rotor speed, torque command/motor torque, and magnitude of $\mathbf{v}^*_{dq\_\rm mdl}$ are depicted from the top to bottom. Here, control mode switching occurred at approximately $t = 0.18$ s and the dc-link voltage was 300 V. Torque distortions are rare during the transition between MVSC and CVC modes.

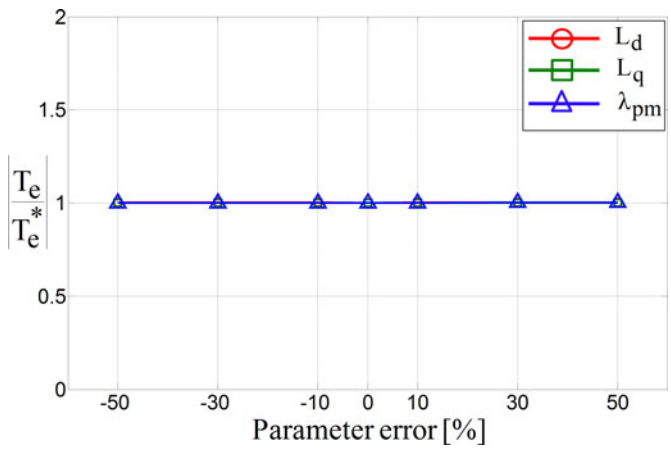

Fig. 12. Torque accuracy with proposed parameter drifts compensation in the MVSC mode.

In Fig. 11(a), $\lambda_{\rm pm}$ was changed step-wise to $+50\%$ of its nominal value at $t = 0.3$ s. The estimated disturbance voltage was delivered to $\boldsymbol{\beta}^*_{dq\_\rm mdl}$ at $t = 0.6$ s. After 0.6 s, the torque error was reduced to almost zero and $|\mathbf{v}^*_{dq\_\rm mdl}|$ was relocated back to the linear voltage circle. The same test was repeated under $+20\%$ of ΔL_q, as shown in Fig. 11(b).

Fig. 12 presents the steady-state torque error plots under the proposed compensation method within a $\pm 50\%$ error bound. Compared to Fig. 8, the torque was controlled precisely against parameter mismatch because the proposed compensation method provides a concurrent estimation of the magnetic saturation and temperature fall/rise. Therefore, this design can be effective for accurately estimating and compensating for torque deviations while reducing the computational complexity. Fig. 13 shows the control block diagram of the proposed MVSC to compensate for the parameter variation effects in real time. A step change in torque command may result in motor current oscillations in the MVSC mode. In fact, it takes multiple settling steps to achieve a desired air-gap torque that is physically infeasible in a couple of steps because the controller is in the voltage-deficit region. This means that the rapid change of torque command is unnecessary in practice. In this paper, a low-pass filter with a 500 rad/s cutoff frequency is applied to manipulate the torque command.

III. Experimental Results

The proposed hybrid maximum voltage utilization algorithm was implemented on a 900-W IPMSM coupled to a 1.0-kW ac servo motor, as described in Table I. An encoder of 2500-pulse-per-revolution was mounted on one end of the test motor to measure the actual rotor position. Multidimensional map data tables were prepared to perform a robust MTPA operation below the base speed and generate a d-axis current command under flux weakening [12]. The algorithm was implemented in the inverter with a constant PWM switching frequency of 10 kHz and the dc-link voltage was set to 150 V. The coupled servo drive was operated in the speed-control mode, which serves as a gasoline or diesel-powered engine, while a load torque command for the

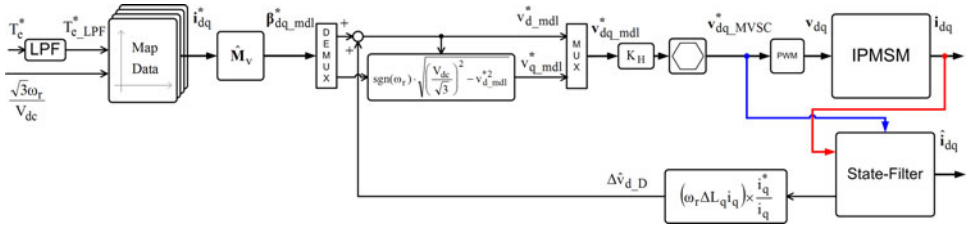

Fig. 13. Block diagram of the proposed MVSC with model error compensation.

TABLE II
SPECIFICATIONS OF TORQUE SENSOR

Specifications	Value	Unit
Supply Voltage	11-16	V_{DC}
Output Range	±10	Nm
Output Voltage	±5	V
Tolerances	±0.1	%

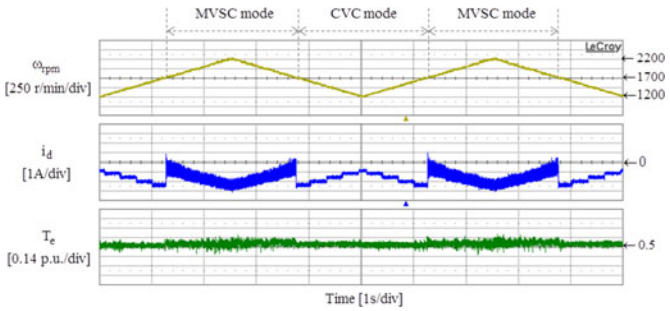

Fig. 14. Control mode switching test result.

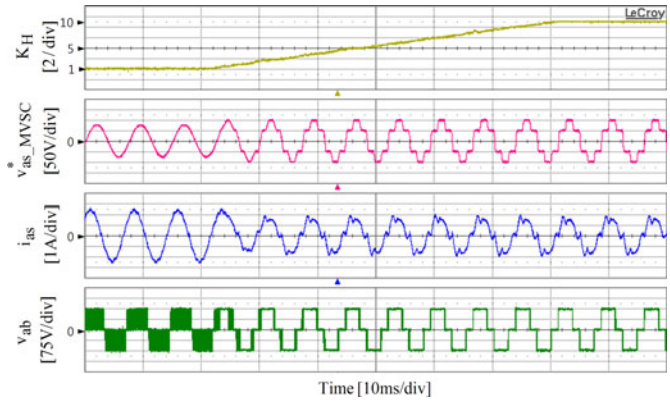

Fig. 15. Transition performance to the full six-step modulation.

driver input command was regulated to the tested IPMSM. The advent of flux weakening occurs at approximately 1700 r/min. A precise torque sensor from Lorenz Messtechnik GMBH with a 1-kHz bandwidth was installed between the IPMSM and the servo motor to measure the real torque, as described in Table II. The online disturbance state filter was performed every 50 μs and its bandwidth was set to 2000 rad/s [16].

Fig. 14 shows the controller switching performance between the CVC and MVSC modes. From the top to bottom, the rotor speed, d-axis current, and the torque measured by the torque sensor are depicted. In this test, all the motor parameters were changed intentionally to +20% of its nominal value. The speed command was varied from 1200 and 2200 r/min with the mode switching speed set to 1700 r/min. The scalar gain K_H was set to 1 in the CVC mode and adjusted to 2 to deliver the modulating voltage to the overmodulation region. In the speed acceleration period, the d-axis current of the CVC mode fell steadily to perform the MTPA operation and was increased at the mode switching instant because the stator voltage is increased to the hexagon. Torque distortions were rarely found during the transition between MVSC and CVC modes. The smooth transition could be achieved simply by resetting the CVC integrator at the control switching instant, as mentioned in Fig. 6. The torque was controlled precisely under the motor parameter variation because the proposed state-filter design provides a concurrent compensation.

To examine the transition performance into the full six-step modulation, the scalar gain K_H was increased from 1 to 10 at 2200 r/min, as shown in Fig. 15. From the top to bottom, the figures shows the K_H value, A-phase voltage command, A-phase current, and measured motor terminal voltage. A smooth transition was achieved without any discontinuity. Average torque control is still possible in the case of the six-step voltage pattern. This can never be achieved in existing CVC schemes.

A comparative test was performed when the speed command changes from 0 to 2200 r/min to investigate the impact of the stator current magnitude, as shown in Fig. 16. The rotor speed, d-axis current, q-axis current, and stator current envelope are depicted from the top to bottom. Compared to the case of the CVC mode alone [see Fig. 16(a)], the d-axis current amplitude of the MVSC mode [see Fig. 16(b)] was smaller owing to the maximum voltage excitation, whereas the q-axis currents were similar. The tested IPMSM delivered a half-rated torque at 500 r/min and mode switching in Fig. 16(b) occurs at $t = 5.4$ s. The measured torque in the bottom plot of Fig. 16(b) was well regulated because the voltage vector slides on the constant torque curve, as explained in Fig. 7. Consequently, under this test condition, the proposed MVSC achieved a 33% decrease in the stator current magnitude over the CVC mode alone.

The waveforms in Fig. 17 show a full torque response of the proposed MVSC, while the speed command was given as 2000 r/min. From the top to bottom, the rotor speed, the magnitude of $\mathbf{v}^*_{dq\_\mathrm{MVSC}}/\mathbf{v}^*_{dq\_\mathrm{mdl}}$, the low-pass filtered torque command, and the air-gap torque are depicted. As soon as the torque

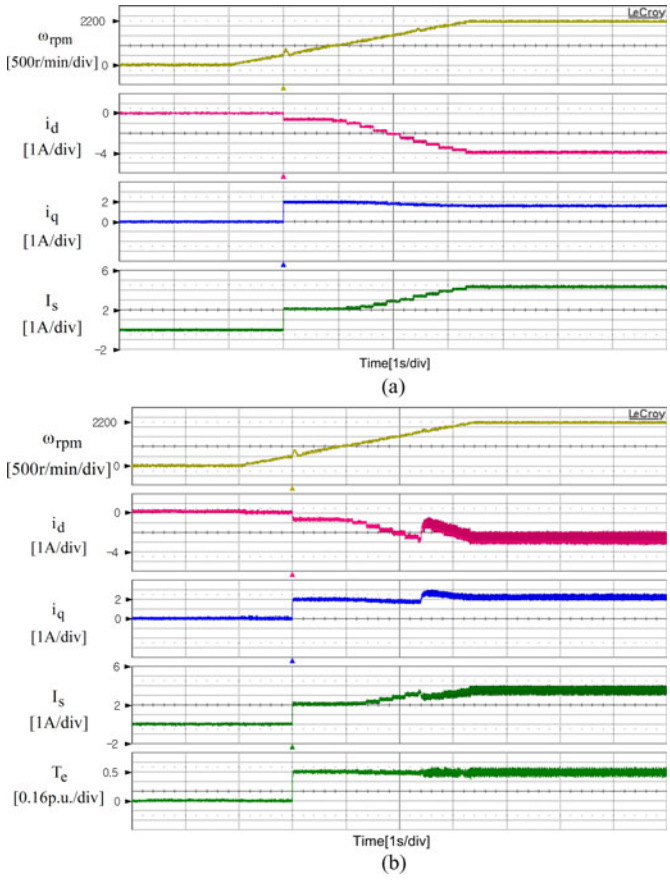

Fig. 16. Comparison of the CVC mode and the proposed hybrid control. (a) CVC mode alone. (b) Proposed hybrid maximum voltage utilization control.

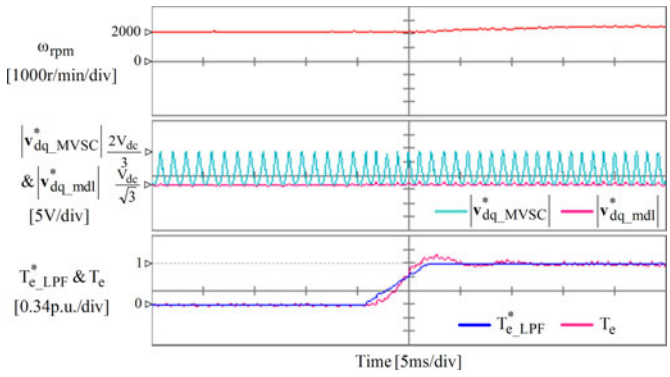

Fig. 17. Full torque test results.

command is applied, the rotor speed starts increasing while the actual torque tracks the torque command. It can be observed that $\mathbf{v}_{dq\_\mathrm{mdl}}^{s^*}$ stays on the voltage circle with a radius of $\frac{V_{\mathrm{dc}}}{\sqrt{3}}$ and $\mathbf{v}_{dq\_\mathrm{MVSC}}^{*}$ extends to the hexagon limit. The result fully illuminates the fact that the proposed method achieves a reliable torque command tracking in the transient state.

The resulting controller works without control interactions resulting from integrators in the PI_CVC and the complex gain tuning process to the full six-step modulation. The test results clearly show that the proposed hybrid control can enhance the power density of the installed inverter capacity and maximize the available battery voltage utilization for electrified vehicle applications.

IV. Conclusion

A combined control structure of IPMSMs for achieving true maximum voltage utilization is proposed. The hybrid structure provides a smooth transition from the CVC to the proposed MVSC mode by deactivating the current regulator in the flux weakening region. A seamless transition to the full six-step modulation can be realized by adjusting the scaling gain, which can be considered a very significant merit in terms of power utilization for wide flux weakening applications. The torque control accuracy under motor parameter drifts is also examined to decouple its influence using a voltage disturbance state filter. The steady-state torque control accuracy is comparable to that of the CVC under the entire operating condition. A comparison with a conventional CVC scheme shows that the proposed MVSC approach can offer minimum copper loss operation over the entire operating range.

Acknowledgment

The operating system and word processing software, ms Windows XP 2002 and MS Word 2007, are used in this paper.

References

[1] I. Husain, *Electric and Hybrid Vehicles Design Fundamentals*. London, U.K.: CRC Press, 2003.
[2] S. R. Macminn and T.M. Jahns, "Control techniques for improved high-speed performance of interior PM synchronous motor drives," *IEEE Trans. Ind. Appl.*, vol. 27, no. 5, pp. 997–1004, Sep./Oct. 1991.
[3] M. A. Rahman and M. A. Masrur, "Advances on IPM technology for hybrid electric vehicles," in *Proc. IEEE Vehicle Power Propulsion Conf.*, Sep. 2009, pp. 92–97.
[4] E. C. Lovelace, T. M. Jahns, and J. H. Lang, "Impact of saturation and inverter cost on interior PM synchronous machine drive optimization," *IEEE Trans. Ind. Appl.*, vol. 36, no. 3, pp. 723–729, May/Jun. 2000.
[5] B. Asaei and B. Rahrovi, "Minimum-copper-loss control over full speed range of an IPMSM drive for hybrid electric vehicle application," in *Proc. IEEE Vehicle Power Propulsion Conf.*, Sep. 2010, pp. 1–6.
[6] I. Aharon and A. Kuperman, "Topological overview of powertrains for battery-powered vehicles with range extenders," *IEEE Trans. Power Electron.*, vol. 26, no. 3, pp. 868–876, Mar. 2011.
[7] Y. S. Jeong, S. K. Sul, S. Hiti, and K. M. Rahman, "Online minimum-copper-loss control of an interior permanent-magnet synchronous machine for automotive applications," *IEEE Trans. Ind. Appl.*, vol. 42, no. 5, pp. 1222–1229, Sep./Oct. 2006.
[8] S. M. Sue and C. T. Pan, "Voltage-constraint-tracking-based field-weakening control of IPM synchronous motor drives," *IEEE Trans. Ind. Electron.*, vol. 55, no. 1, pp. 340–347, Jan. 2008.
[9] T. S. Kwon, G. Y. Choi, M. S. Kwak, and S. K. Sul, "Novel flux-weakening control of an IPMSM for quasi-six-step operation," *IEEE Trans. Ind. Appl.*, vol. 44, no. 6, pp. 1722–1731, Nov./Dec. 2008.
[10] B. Cheng and T. R. Tesch, "Torque feedforward control technique for permanent-magnet synchronous motors," *IEEE Trans. Ind. Electron.*, vol. 57, no. 3, pp. 969–974, Mar. 2010.
[11] A. Consoli, G. Scarcella, G. Scelba, and A. Testa, "Steady-state and transient operation of IPMSMs under maximum-torque-per-ampere control," *IEEE Trans. Ind. Appl.*, vol. 46, no. 1, pp. 121–129, Jan./Feb. 2010.
[12] G. B. Kang, J. S. Lim, K. H. Nam, H. B. Ihm, and H. G. Kim, "A MTPA control scheme for an IPM synchronous motor considering magnet flux variation caused by temperature," in *Proc. IEEE Appl. Power Electron. Conf. Exp.*, 2004, pp. 1617–1621.

[13] J. K. Seok, J. S. Kim, and S. K. Sul, "Overmodulation strategy for high performance torque control," *IEEE Trans. Power Electron.*, vol. 13, no. 4, pp. 786–792, Jul. 1998.
[14] A. M. Hava, S. K. Sul, R. J. Kerkman, and T. A. Lipo, "Dynamic overmodulation characteristics of triangle intersection PWM methods," *IEEE Trans. Ind. Appl.*, vol. 35, no. 4, pp. 896–907, Jul./Aug. 1999.
[15] H. Kim, M. C. Harke, and R. D. Lorenz, "Sensorless control of interior permanent-magnet machine drives with zero-phase lag position estimation," *IEEE Trans. Ind. Appl.*, vol. 39, no. 6, pp. 1726–1733, Nov./Dec. 2003.
[16] S. H. Kim, C. H. Choi, and J. K. Seok, "Voltage disturbance state-filter design for precise torque-controlled interior permanent magnet synchronous motors," in *Proc. IEEE Energy Convers. Congr. Exp.*, 2011, pp. 2445–2451.

SeHwan Kim (S'10) received the B.S. degree from Yeungnam University, Gyeongsan, Korea, in 2010, where he is currently working toward the combined M.S./Ph.D. degree in the Power Conversion Laboratory.

His current research interests include high-performance electrical machine drives, battery voltage maximum utilization for EVs/HEVs, and precise torque control of PM synchronous motors.

Jul-Ki Seok (S'94–M'98–SM'09) received the B.S., M.S., and Ph.D. degrees from Seoul National University, Seoul, Korea, in 1992, 1994, and 1998, respectively, all in electrical engineering.

From 1998 to 2001, he was a Senior Engineer with the Production Engineering Center, Samsung Electronics, Suwon, Korea. Since 2001, he has been a member of the faculty of the School of Electrical Engineering, Yeungnam University, Gyeongsan, Korea, where he is currently a Professor. His research interests include motor drives, power converter control of offshore wind farms, and nonlinear system identification related to the power electronics field.

Dr. Seok serves as the Chair of the IEEE Industry Applications Society Industrial Drive Committee Paper Award Subcommittee, an Associate Editor of the IEEE TRANSACTIONS ON INDUSTRY APPLICATIONS, and the Editorial Board of the *IET Electric Power Applications*.